Vol 15 No 7, July 2006
1009-1963/2006/15(07)/1549-09

Chinese Physics

© 2006 Chin. Phys. Soc.
and IOP Publishing Ltd

A comparative study of the structure and crystallization of bulk metallic amorphous rod $Pr_{60}Ni_{30}Al_{10}$ and melt-spun metallic amorphous ribbon $Al_{87}Ni_{10}Pr_3$*

Meng Qing-Ge(孟庆格)†, Li Jian-Guo(李建国), and Zhou Jian-Kun(周建坤)

School of Materials Science and Engineering, Shanghai Jiaotong University, Shanghai 200030, *China*

(Received 9 October 2005; revised manuscript received 4 April 2006)

Pr-based bulk metallic amorphous (BMA) rods ($Pr_{60}Ni_{30}Al_{10}$) and Al-based amorphous ribbons ($Al_{87}Ni_{10}Pr_3$) have been prepared by using copper mould casting and single roller melt-spun techniques, respectively. Thermal parameters deduced from differential scanning calorimeter (DSC) indicate that the glass-forming ability (GFA) of $Pr_{60}Ni_{30}Al_{10}$ BMA rod is far higher than that of $Al_{87}Ni_{10}Pr_3$ ribbon. A comparative study about the differences in structure between the two kinds of glass-forming alloys, superheated viscosity and crystallization are also made. Compared with the amorphous alloy $Al_{87}Ni_{10}Pr_3$, the BMA alloy $Pr_{60}Ni_{30}Al_{10}$ shows high thermal stability and large viscosity, small diffusivity at the same superheated temperatures. The results of x-Ray diffraction (XRD) and transmission electron microscope (TEM) show the pronounced difference in structure between the two amorphous alloys. Together with crystallization results, the main structure compositions of the amorphous samples are confirmed. It seems that the higher the GFA, the more topological type clusters in the Pr–Ni–Al amorphous alloys, the GFAs of the present glass-forming alloys are closely related to their structures.

Keywords: Pr–Ni–Al amorphous alloys, amorphous structure, crystallization, glass-forming ability (GFA)

PACC: 6000, 6155H

1. Introduction

Amorphous metallic alloys have unique mechanical and physical properties attributed to the atomic structure of the amorphous phase. Recently, a class of Al–TM–RM (the TM stands for transition metal, RM for rare earth metal) ternary amorphous alloys with a wide range of glass-forming compositions have attracted much attention due to their excellent specific strength, large coercive fields, etc.[1−4] In this system, the high cooling rates, above 10^5 K/s, are generally required to produce the Al-based amorphous alloys and the 'bulk' Al-based amorphous alloys made by quenching a liquid, which are only about 140 μm in thickness up to now. On the contrary, the RM-based amorphous alloys can be easily made up to 6 mm in diameter by a conventional casting process at much lower critical cooling rates ($\leq 10^2$ K/s). Since the discovery of amorphous alloys, a number of attempts have been made to understand the mechanism of amorphization in order to predict alloy compositions with better glass-forming ability (GFA). Inoue[5] proposed three empirical rules to find high GFA in metallic glass-forming systems. Mukherjee *et al* [6] studied the viscosity and specific volume of Zr-based bulk metallic glass-forming alloys (BMG) which indicated that the better glass former had high viscosity at its liquidus temperature and showed a small change in volume upon crystallization compared with a poorer glass former. Furthermore, based on the concept of dense random packing (DRP) of atoms, structures of amorphous alloys with chemical and topological atomic short-range order (SRO) and medium-range order (MRO) of atoms have been studied in order to understand the mechanism of amorphization details and magnetic characteristics.[7,8] Generally, SRO is in the range 3–5Å while the MRO is in the range 5–20Å.[9,10] Topological complexity and frustration were given in Ref.[11] as an explanation of suppression crystallization in multicomponent alloys. However, the intrinsic characters of the different GFA alloys, especially with the same element compositions have not been studied yet and further investigations are needed.

In view of the above considerations, it seems attractive to pursue a comparative study on the structure, viscosity and crystallization of the ordi-

*Project supported by the National Science Foundation for Outstanding Young Scientists of China (Grant No 50125101).
†E-mail: mggsjtu@sjtu.edu.cn

nary amorphous alloy $Al_{87}Ni_{10}Pr_3$ and BMA alloy $Pr_{60}Ni_{30}Al_{10}$, which are the same in component element but quite different in GFA. In this study, the structure parameters such as coordination numbers (N), the nearest interatomic distance r_1, the correlation radius of clusters r_c etc are calculated and compared with the continuously heated XRD crystallization data. The diffusion parameters and apparent activation energies (E_v) of viscous flows in $Al_{87}Ni_{10}Pr_3$ and $Pr_{60}Ni_{30}Al_{10}$ melts during solidification are also calculated from the viscosity data by using the modified Stokes–Einstein equation, Arrhenius equation [12−15] and Cohen–Grest model.[16] This paper clarifies the factors related to the mechanism of amorphization from a different point of view and offers important clues to understand the essence of GFA.

2. Experiment

Alloys with nominal atomic percent compositions of $Al_{87}Ni_{10}Pr_3$ and $Pr_{60}Ni_{30}Al_{10}$ were prepared by arc melting Al, Ni (both with the purity of no less than 99.9 wt.%) and Pr (with the purity of no less than 99.7 wt.%) in titanium-gettered argon atmosphere. $Al_{87}Ni_{10}Pr_3$ amorphous ribbons were produced by the single roller melt-spun technique in an argon atmosphere. The copper roller was 35 cm of diameter and typically 20 m/s of circumferential velocity. The ribbons were 2–4 mm in width and 20–30 μm in thickness. Cylindrical specimens of 3 mm in diameter and 80 mm in length were prepared from the $Pr_{60}Ni_{30}Al_{10}$ pre-alloys ingots by suction casting into a copper mould and the anneal was carried out in an evacuated quartz tube.

The temperature-dependent viscosities for the samples in a liquid state were measured using an oscillating vessel viscometer (RHEOTRONI C Ⅷ) during cooling. The superheating temperature of the melts ranges from about 400 K to 100 K. At each temperature the melt was allowed to equilibrate for 20 min before measurement. The samples were placed in a purified argon atmosphere. The experiments were carried out four to seven times at every temperature and the measured values were averaged. Schvidkovskii's equation[17] was used to calculate the viscosity from the measured damping data.

Thermal analysis was performed with a Netzsch DSC 404C calorimeter. All the DSC measurements were conducted in a flowing (60 cm^3/min) argon gas; The amorphous state of the cast cylinders was examined by XRD in a D/Max-rB diffractometer using Cu-Kα radiation, the scattering angle (2θ) range is in 5°–100°. The detailed treatment of the scattering intensity measured in arbitrary units has been described in Refs.[18,19] according to which, the structure factor $S(Q)$ ($Q = (4\pi \sin\theta/\lambda)$ is the magnitude of the scattering vector and λ is the wavelength.) then the pair distribution function (PDF) and radial distribution function (RDF) can be calculated by programming. The microstructure was further investigated by a TEM HITACHI-800.

3. Results and discussion

3.1. Amorphous structure of $Al_{87}Ni_{10}Pr_3$ ribbon and $Pr_{60}Ni_{30}Al_{10}$ BMA rod

Figure 1(a) shows the XRD patterns of $Al_{87}Ni_{10}Pr_3$ ribbons and as-cast $Pr_{60}Ni_{30}Al_{10}$ rods each with a diameter of 3 mm. The samples exhibit a series of broad diffraction maximum characteristics of metallic glass with no evidence of a crystalline Bragg peaks, indicating the formation of a single amorphous phase. The total structure factors of $Al_{87}Ni_{10}Pr_3$ amorphous ribbons and $Pr_{60}Ni_{30}Al_{10}$ BMA rods at room temperature are shown in Fig.1(b). For $Al_{87}Ni_{10}Pr_3$ amorphous ribbons, a distinct prepeak occurs at Q=10–20nm^{-1}, which is believed to be a characteristic of MRO in amorphous alloys [20,21] and the structure size of MRO can be estimated by the expression $R_{MRO}=2\pi/Q_{pp}$, where Q_{pp} is the position of the prepeak.[21] The ratio of the prepeak area to the total area of the main peak and the prepeak in the x-ray intensity curve, $S_{prepeak}/S_{total}$, reflects the proportion of the structure corresponding to the prepeak in the matrix. The values of R_{MRO} and $S_{prepeak}/S_{total}$ are listed in Table 1. For $Pr_{60}Ni_{30}Al_{10}$ BMA rods, no prepeak can be found in Figs.1(a) and 1(b). However, the pronounced structure at higher angles is a feature for $Pr_{60}Ni_{30}Al_{10}$ BMA rod that is not present in the patterns of $Al_{87}Ni_{10}Pr_3$ amorphous ribbon. This feature can also be seen clearly from the corresponding RDFs shown in Fig.1(c) and PDFs shown in Fig.1(d). At higher XRD angles (i.e. at farther distance from the reference atom), the RDF and PDF curve swings of $Pr_{60}Ni_{30}Al_{10}$ BMA rod are bigger than those of $Al_{87}Ni_{10}Pr_3$ amorphous ribbon, indicating higher packing fraction and larger relative cluster radius, respectively. The difference in structure between the two kinds of amorphous alloys will be thoroughly discussed along with the crystallization process in Section 3.3.

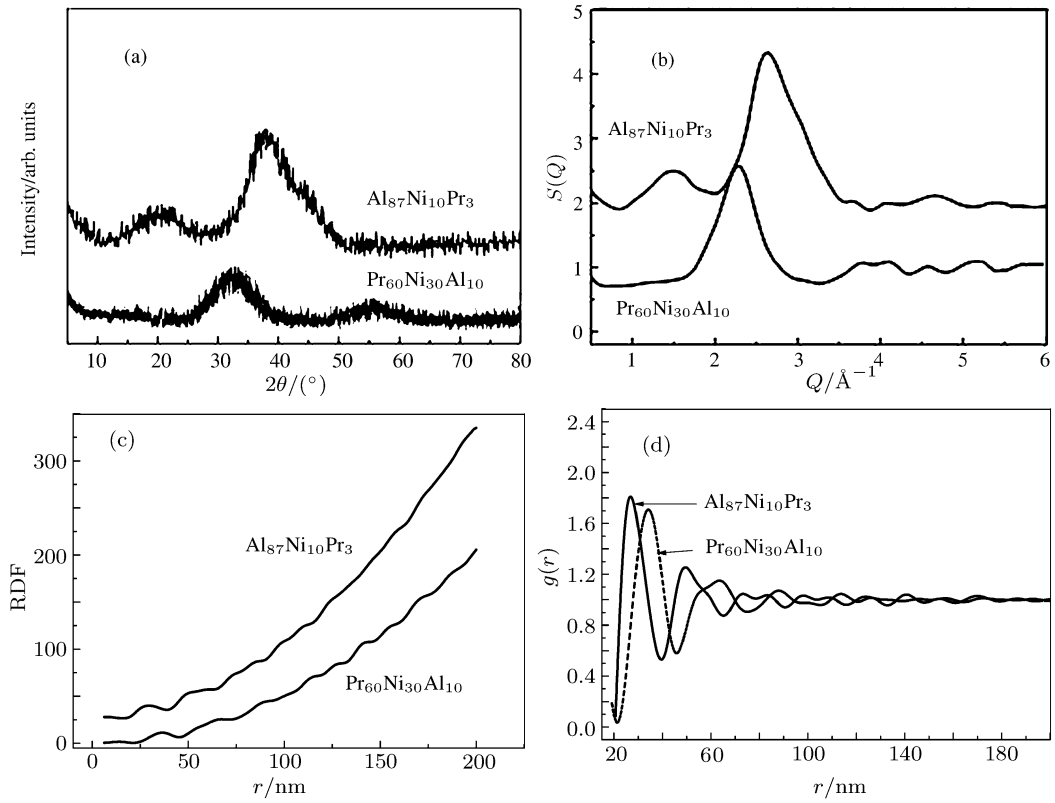


Fig.1. (a) XRD patterns and calculated results of structure parameters; (b) total structure factor $S(Q)$; (c) radical distribution functions (RDF); and (d) pair distribution functions (PDF) of $Al_{87}Ni_{10}Pr_3$ ribbons and as-cast $Pr_{60}Ni_{30}Al_{10}$ rods each with a diameter of 3 mm.

Table 1. Summary of the amorphous structure parameters: MRO size $R_{\rm MRO}$, MRO structure ratio $S_{\rm prepeak}/S_{\rm total}$, nearest-neighbour atom distance r_1, average atom distance of displacement σ, coordination number of nearest-neighbour atoms N_1, relative cluster radius $r_{\rm c}$ and atom number of relative cluster $N_{\rm c}$.

Amorphous alloys	$R_{\rm MRO}$/Å	$S_{\rm prepeak}/S_{\rm total}$	r_1/Å	N_1	σ/Å	$r_{\rm c}$/Å	$N_{\rm c}$
$Al_{87}Ni_{10}Pr_3$	4.21	0.200	2.680	12.436	0.395	14.031	750.28
$Pr_{60}Ni_{30}Al_{10}$	—	—	3.398	13.250	0.489	17.421	906.13

The parameters deduced from Figs.1(c) and 1(d) to evaluate the amorphous structure are mainly nearest-neighbour atom distance r_1, average atom distance of displacement σ, coordination number of nearest-neighbour atoms N_1, relative cluster radius $r_{\rm c}$ and atomic number of relative cluster $N_{\rm c}$. r_1 is the position of the first peak on PDF curve and the coordination number N_1 is the area under the first peak of RDF curve. σ is a parameter to evaluate the degree of static randomness and thermodynamic vibration of amorphous structure, which can be calculated from the peak width of the RDF curve. $r_{\rm c}$ is determined from the following equation:

$$\left|\frac{\rho(r)-\rho_0(r)}{\rho_0(r)}\right| \geq k_{\rm c}, \qquad (1)$$

where $\rho(r)$ is the atom density function, $\rho_0(r)$ is the average atom density function and $k_{\rm c}$ is 0.01. $N_{\rm c}$ is the integration of the RDF curve from 0 to $r_{\rm c}$. All the structure parameters are listed in Table 1.

As can be seen from Table 1, for the ternary amorphous alloys, the nearest-neighbour atom distance r_1 calculated is between the interatomic distances of the two dominant elements (metallic radius (Å) for atoms with coordination number (CN) CN=12, $r_{\rm Al}$= 1.432, $r_{\rm Ni}$= 1.246, $r_{\rm Pr}$=1.828). The coordination number of nearest-neighbour atoms N_1 (12.436) of $Al_{87}Ni_{10}Pr_3$ amorphous ribbon is smaller than that (13.250) of $Pr_{60}Ni_{30}Al_{10}$ BMA rod, indicating $Pr_{60}Ni_{30}Al_{10}$ BMA alloy has a more condensed structure and higher packing fraction. The average atom distance of displacement σ shows that the amorphous structure of $Pr_{60}Ni_{30}Al_{10}$ is stabler than that of $Al_{87}Ni_{10}Pr_3$ amorphous ribbon and this is also confirmed by the crystallization experiments later. The relative cluster radius $r_{\rm c}$ of $Pr_{60}Ni_{30}Al_{10}$ BMA rod is 17.421Å, which is much

bigger than that of $Al_{87}Ni_{10}Pr_3$ amorphous ribbon, and this value has the same magnitude as that of the SRO structures discovered by Fan *et al* in Nd–Fe–Al BMA alloys.[22]

3.2. Viscosity and diffusivity of superheated melts

Figure 2 shows the changes of viscosities of liquid $Pr_{60}Ni_{30}Al_{10}$ and $Al_{87}Ni_{10}Pr_3$ as a function of temperature.

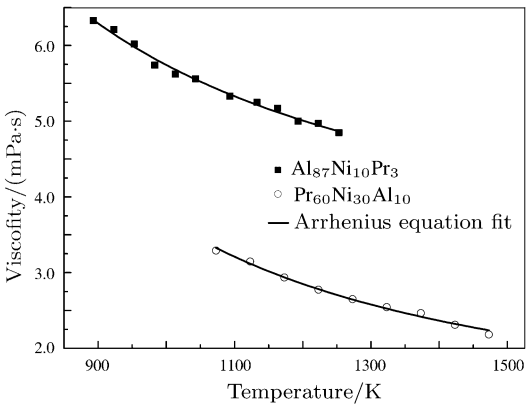


Fig.2. Viscosities of $Pr_{60}Ni_{30}Al_{10}$ and $Al_{87}Ni_{10}Pr_3$ alloys with superheating temperatures.

The corrected Arrhenius equation fitting curves are also given below, which describe the temperature-dependence of liquid viscosity:[23]

$$\eta = A\,\exp(E_{\rm v}/k_{\rm B}T),\ A = h/v_{\rm m}, \tag{2}$$

where η is the viscosity, $k_{\rm B}$ is the Boltzmann constant, h is Planck's constant, T is the absolute temperature, $v_{\rm m}$ is the flow unit-volume, and $E_{\rm v}$ is the activation energy that is the energy required to move flow unit-volume from one balanced position to another one in melt. The values of $v_{\rm m}$ and $E_{\rm v}$ for $Pr_{60}Ni_{30}Al_{10}$ and $Al_{87}Ni_{10}Pr_3$ are respectively 2.622 × 10^{-26} cm^3, 0.0707 eV and 8.576 × $10^{-25}cm^3$, 0.135 eV. If the flow unit-volume of $Pr_{60}Ni_{30}Al_{10}$ liquid is the same as that of $Al_{87}Ni_{10}Pr_3$ melt, the activation energy of $Pr_{60}Ni_{30}Al_{10}$ liquid may be approximately calculated by the following formula:

$$E_{\rm vPr}{}_E = \frac{v_{\rm mAl}}{v_{\rm mPr}} \times E_{\rm vPr}, \tag{3}$$

where $E_{\rm vPr}{}_E$ is the activation energy that is the energy required to move the same unit-volume as that of $Al_{87}Ni_{10}Pr_3$ liquid (here $v_{\rm mAl}$ is 8.576 × 10^{-25} cm^3). $v_{\rm mAl}$, $v_{\rm mPr}$ and $E_{\rm vPr}$ are the respectively $Al_{87}Ni_{10}Pr_3$ flow unit, $Pr_{60}Ni_{30}Al_{10}$ flow unit and $Pr_{60}Ni_{30}Al_{10}$ activation energy calculated from the formula (2), respectively. Thus the value of $E_{\rm vPr}{}_E$ is 2.312 eV that is about sixteen times bigger than that of $Al_{87}Ni_{10}Pr_3$. The atom movement in $Pr_{60}Ni_{30}Al_{10}$ is very difficult compared with that in $Al_{87}Ni_{10}Pr_3$.

Sutherland (1905) made a correction in the Stokes–Einstein equation by using hydrodynamic theory:[12]

$$D = \frac{kT}{6\pi\eta r}\frac{1+3\eta/\beta_{\rm s}r}{1+2\eta/\beta_{\rm s}r}, \tag{4}$$

where k is the Boltzmann constant, T is the absolute temperature, r is the radius of the diffusing particles and $\beta_{\rm s}$ is the coefficient of sliding friction between the diffusing particle and medium, which depends on the size of the medium. When the diffusing particle is large in radius, compared with the particles of the medium, $\beta_{\rm s}$ equals infinity. When the radius of the diffusing particle is approximately equal to that of the medium particles, $\beta_{\rm s}$ becomes zero. In the cases of $Pr_{60}Ni_{30}Al_{10}$ and $Al_{87}Ni_{10}Pr_3$ alloys, $\beta_{\rm s}$ is approximately zero, r is assumed to be nearest-neighbour atom distance r_1. Therefore Eq.(4) may be written as

$$D = \frac{kT}{4\pi\beta r_1}, \tag{5}$$

Then inserting Eq.(2) into Eq.(5) yields

$$D_{\rm Al_{87}Ni_{10}Pr_3} = 1.665\times10^{-11}T\,\exp\left(\frac{-1566.603}{T}\right), \tag{6}$$

$$D_{\rm Pr_{60}Ni_{30}Al_{30}} = 1.227\times10^{-12}T\,\exp\left(\frac{-820.932}{T}\right). \tag{7}$$

Diffusivities obtained from Eqs.(6) and (7) are shown in Fig.3 together with diffusivities of pure Al and Ni for a comparison, which that were predicted by Protopapas *et al* in 1973. It is obvious that the diffusivities of $Al_{87}Ni_{10}Pr_3$ alloys are much bigger than those of $Pr_{60}Ni_{30}Al_{10}$ alloys at the same superheating temperatures. Thus high viscosity and correspondingly low diffusivity of the liquid contribute significantly to high GFA of $Pr_{60}Ni_{30}Al_{10}$.

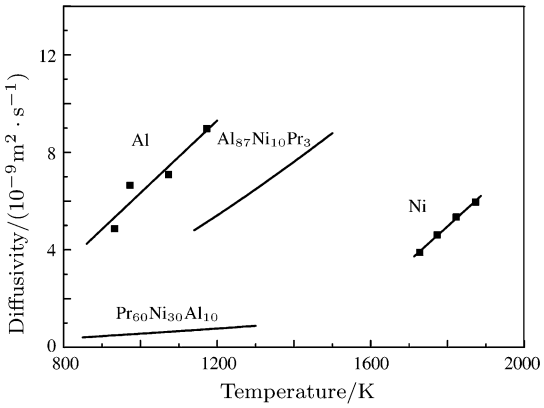


Fig.3. Diffusivities of $Pr_{60}Ni_{30}Al_{10}$ and $Al_{87}Ni_{10}Pr_3$ together with the diffusivities of pure Al and Ni[24] for a comparison at superheating temperatures.

3.3. Crystallization of $Al_{87}Ni_{10}Pr_3$ ribbon and $Pr_{60}Ni_{30}Al_{10}$ BMA rod

Crystallization studies of the metallic glass are of importance in understanding the amorphous structures, the mechanism of phase transformations and the GFA of the alloys.[25] Figure 4 shows the DSC traces of the $Pr_{60}Ni_{30}Al_{10}$ BMA rods and $Al_{87}Ni_{10}Pr_3$ amorphous ribbons at different heating rates of 5, 10, 20, 30 and 50 K/min, respectively. It can be seen that the crystallization peak shifts toward higher temperatures with the increase of heating rate, indicating the obvious kinetic behaviour of crystallization.

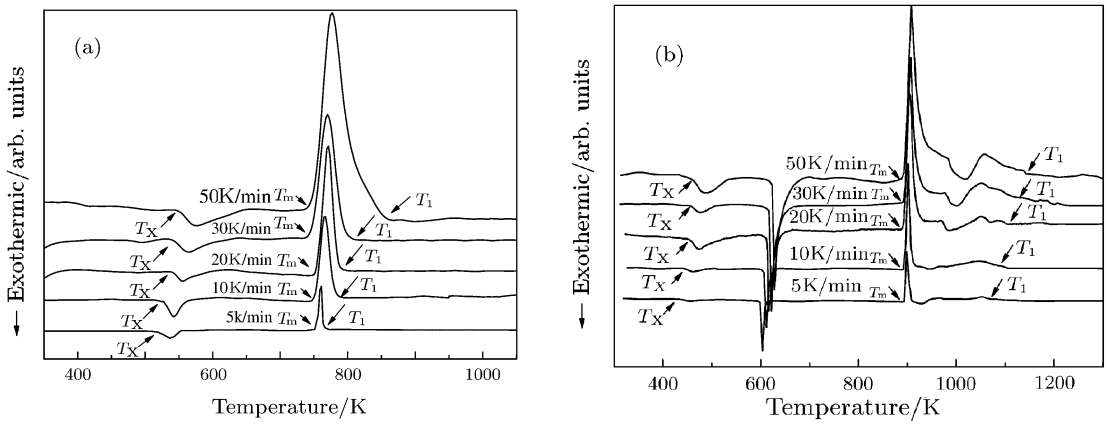


Fig.4. DSC traces for (a) $Pr_{60}Ni_{30}Al_{10}$ BMA rods and (b) $Al_{87}Ni_{10}Pr_3$ amorphous ribbons at different heating rates from 5 to 50 K/min.

Table 2. Thermal properties deduced from the DSC measurements at a heating rate of 20 K/s, the onset temperatures of crystallization T_x, onset melting temperatures T_m, offset melting temperatures T_1, GFA indicators T_x/T_1, and γ, for $Pr_{60}Ni_{30}Al_{10}$ BMA rod and $Al_{87}Ni_{10}Pr_3$ amorphous ribbon. As the glass transition temperatures T_g of the two alloys cannot be found, T_x is used instead.

Alloys	Sample size/mm	T_x/K	T_m/K	T_1/K	T_x/T_1	γ
$Pr_{60}Ni_{30}Al_{10}$	Φ 3 × 80	541.6	748	784.3	0.690	0.410
$Al_{87}Ni_{10}Pr_3$	2 × 0.030	442.1	892	1114	0.397	0.284

If the parameters (listed in Table 2) of T_{rx} ($=T_x/T_1$)[26] and γ ($(=T_x/(T_g+T_1))$[27] are adopted to evaluate the GFAs of the two kinds of samples, the GFA of $Pr_{60}Ni_{30}Al_{10}$ alloys is far larger than that of $Al_{87}Ni_{10}Pr_3$ alloys. Further, the crystallization kinetics of the amorphous alloys is evaluated using Kissinger's equation[27] in the following form:

$$\ln\left(\frac{T_x^2}{\phi}\right) = \ln\left(\frac{E_x}{k_B K_0}\right) + \frac{E_x}{k_B T_x}, \qquad (8)$$

where ϕ is the heating rate, T_x denotes the onset temperature of the glass transition or crystallization, k_B the Boltzmann constant (k_B=8.6173585 × 10^{-5} eV·K^{-1}) and E_x the apparent activation energy of crystallization. K_0 is the frequency factor in the Arrhenius law, that is, $K_T = K_0 \exp(-E/k_BT)$. Kissinger plot of T_x is shown in Fig.5. The values of E_x and K_0 of the crystallization obtained from the Kissinger method are 1.585 eV and 3.765 × 10^{12} s^{-1} for $Pr_{60}Ni_{30}Al_{10}$, and 1.287 eV and 5.909 × 10^{12}s^{-1} for $Al_{87}Ni_{10}Pr_3$. The apparent activation energy E_x can be interpreted as the additional energy that an atom must acquire in order to be a part of the activated cluster.[28] $Pr_{60}Ni_{30}Al_{10}$ BMA rod shows a higher value of E_x, i.e. its amorphous structure has the better thermal stability than $Al_{87}Ni_{10}Pr_3$ amorphous ribbon. This agrees well with the result deduced

from the structure parameter ρ mentioned in Section 3.1. Further, the evaluation of the rate constant K_T is a way of estimating GFA to some extent.[28] The crystallization reaction rate constant K_{T_x} at T_x is calculated by using the Arrhenius law from K_0, E_x and T_x. At a DSC heating rate of 20 K/min, the calculated rate constants K_{T_x} for $Pr_{60}Ni_{30}Al_{10}$ BMA rod and $Al_{87}Ni_{10}Pr_3$ amorphous ribbon are 6.712 × $10^{-3}s^{-1}$ and 1.260 × 10^{-2} s^{-1} respectively. The sample with a smaller K_x has a better GFA.

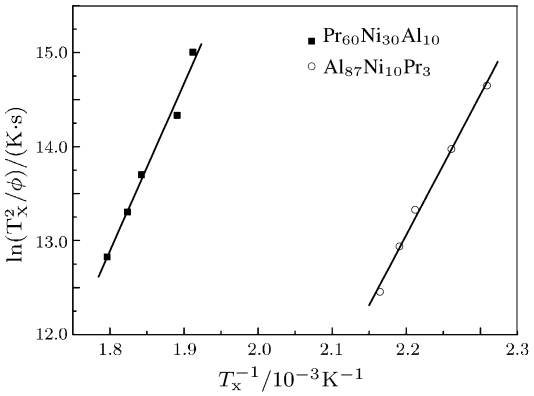


Fig.5. The Kissinger plots of T_x of BMG $Pr_{60}Ni_{30}Al_{10}$ and amorphous ribbon $Al_{87}Ni_{10}Pr3$.

In order to shed more light on the amorphous structure and crystallization of amorphous alloys, the $Pr_{60}Ni_{30}Al_{10}$ rods and $Al_{87}Ni_{10}Pr_3$ ribbons, which each had been heated up to temperatures of different crystallization stages according to their DSC curves, were investigated by XRD and TEM. Figure 6(a) shows XRD patterns of $Pr_{60}Ni_{30}Al_{10}$ BMA rods continuously heated to 545 and 660 K. Crystalline phases formed are indicated by strong peaks representing hexagonal-Pr crystals, and weak peaks representing intermetallics (Pr_7Ni_3, PrNi etc.) at the first crystallization stage of 545 K. By continuously increasing the temperature to 660 K, crystalline phases are the same as those at the first stage according to XRD measurements of the samples continuously heated. Figure 7 shows TEM images of $Pr_{60}Ni_{30}Al_{10}$ sample continuously heated to 660 K (exceeding the crystallization peak temperature), a temperature at which Pr_7Ni_3, PrNi and Pr phases are formed according to the selected-area electron diffraction patterns. This agrees well with the result in Fig.6(a).

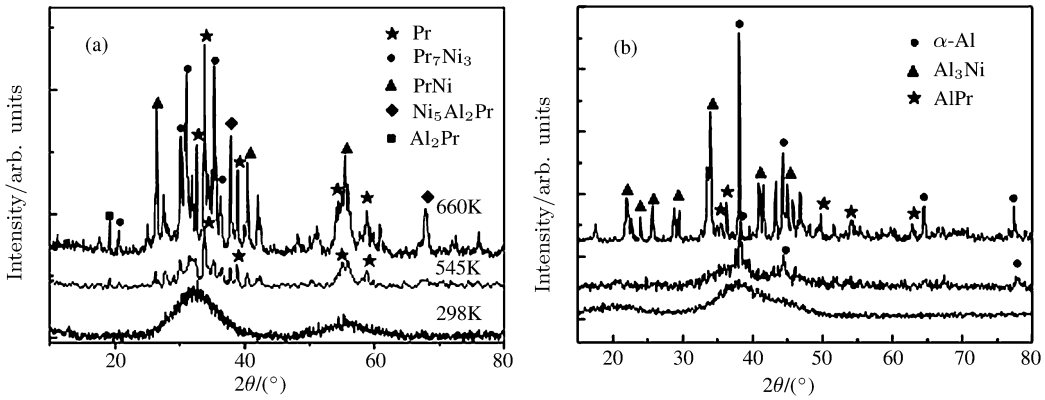


Fig.6. The x-ray patterns of the BMA rods $Pr_{60}Ni_{30}Al_{10}$ (a) and amorphous ribbons $Al_{87}Ni_{10}Pr_3$ (b) continuously heated in the DSC equipment up to the indicated temperature, corresponding to each crystallization stage. The formed crystalline phases are indexed.

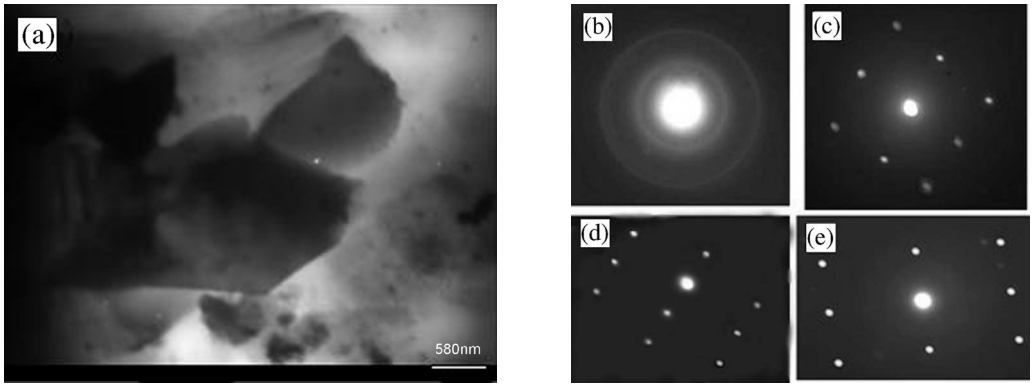


Fig.7. TEM bright-field micrographs of (a) $Pr_{60}Ni_{30}Al_{10}$ continuously heated to 660 K, and corresponding selected-area electron diffraction patterns of (b) nanosized Pr, (c) Pr crystals, (d) PrNi intermetallics, (e) Pr_7Ni_3 intermetallics.

Figure 6(b) shows XRD patterns of amorphous $Al_{87}Ni_{10}Pr_3$ continuously heated to 473 K and 583 K. Unlike that of the $Pr_{60}Ni_{30}Al_{10}$ sample, fcc-Al crystals is formed at the first stage, however other intermetallics, i.e. Al_3Ni, AlPr and additional fcc-Al phases can be detected by XRD and TEM [7] only after the sample has been heated up to 583 K (exceeding the second crystallization peak temperature). As mentioned in Section 3.1, there are obvious differences in amorphous structure between the two kinds of alloys. From Fig.6 it can be seen that Al_3Ni intermetallics spring up from the prepeak position of $Al_{87}Ni_{10}Pr_3$ after crystallization, which results from the strong interactions between Al and Ni atoms. The main peak of $Pr_{60}Ni_{30}Al_{10}$ BMA rod mostly corresponds to the Pr–Pr and Pr–Ni type correlations as Pr_7Ni_3, PrNi and Pr phases spring up from this position by crystallization. Similarly, the main peak of $Al_{87}Ni_{10}Pr_3$ amorphous ribbon reflects strong Al–Al type correlations. In order to dig out the structure relationships between the amorphous alloys and their crystallization counterparts, the RDF Gaussian decompositions of $Pr_{60}Ni_{30}Al_{10}$ BMA rod and $Al_{87}Ni_{10}Pr_3$ amorphous ribbon were made.

According to the Einstein liquid model,[30] and the work of Kita *et al* [31] and Wang *et al*,[32] the reduced distribution function $[4\pi r\rho(r)]$ and RDF $[4\pi r^2\rho(r)]$ of simple liquid can be reasonably decomposed into Gaussian peaks with a separation range of several angstroms. The Gaussian decompositions of RDFs of $Pr_{60}Ni_{30}Al_{10}$ and $Al_{87}Ni_{10}Pr_3$ amorphous samples are shown in Fig.8, where the first two peaks of RDF are decomposed into five and four Gaussian peaks respectively. The first three Gaussian peaks corresponding to the first peak in Fig.1(c) are our concern. The first RDF peak position r_1 is the nearest-neighbour atom distance, and the area under the first RDF peak is coordination number of nearest-neighbour atoms N_1.

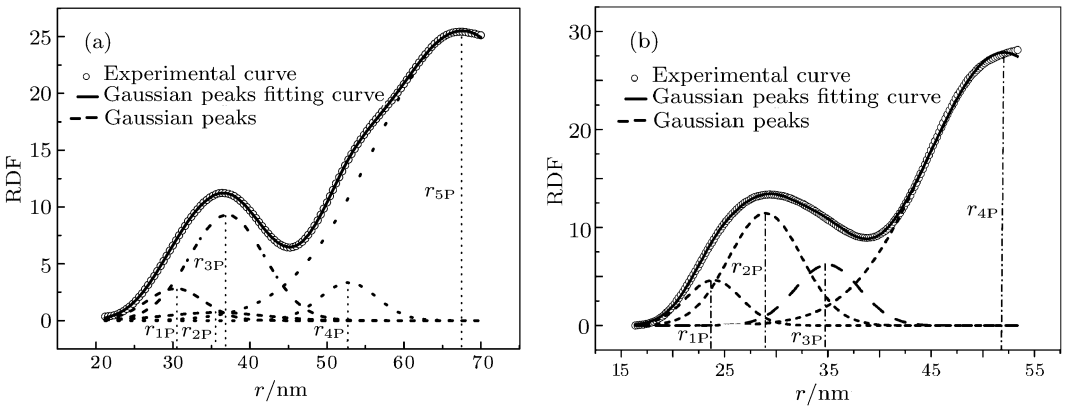


Fig.8. Gaussian decompositions of RDF of (a) $Pr_{60}Ni_{30}Al_{10}$ BMA rod and (b) $Al_{87}Ni_{10}Pr_3$ amorphous ribbon.

The decomposition results are listed in Table 3, the decomposition range for $Pr_{60}Ni_{30}Al_{10}$ BMA alloy is about 0–7 Å and the separation range for $Al_{87}Ni_{10}Pr_3$ is 0–5.5 Å. The former is larger than the latter because the nearest-neighbour atom distance r_1 of $Pr_{60}Ni_{30}Al_{10}$ BMA rod is bigger than that of the $Al_{87}Ni_{10}Pr_3$ amorphous ribbon. The atom correlations for different separated Gaussian peaks are also confirmed according to their peak positions (r_{1p}, r_{2p}, r_{3p}). For $Al_{87}Ni_{10}Pr_3$ amorphous ribbon, there are two kinds of atom correlations. One is dominant atom correlations originating from Al–Al (total 73.18%) clusters, which include 16.98% Al–Al chemical order correlations and 56.20% topological order correlations. The other is Al–Ni chemical order correlation, which corresponds to the Al_3Ni intermetallics of crystallization shown in Fig.6(b). Thus the strong interaction between Al and Ni atoms or the forceful intermetallic compound forming inclination may contribute to the existence of Al–Ni chemical order correlations at prepeak and main peak of $Al_{87}Ni_{10}Pr_3$ amorphous ribbon. Because of the very low concentrations of Pr, it is reasonable to find no separated Gaussian peaks corresponding to Al–Pr correlations, notwithstanding there appear several weak peaks indexed as AlPr intermetallics in Fig.6(b). In the case of $Pr_{60}Ni_{30}Al_{10}$ BMA rod, there are mainly three kinds of atom correlations, i.e. Pr–Pr, Pr–Ni topological SRO clusters and Al–Ni–Pr(e.g intermetallics Al_5Ni_2Pr) chemical SRO clusters, of which s_2 of Pr–Pr atom correlation is the largest (75.00%). As far as the first peak of RDF is concerned, the fraction of topolog-

ical type clusters in $Pr_{60}Ni_{30}Al_{10}$ BMA rod is about 36.25 percent larger than that of $Al_{87}Ni_{10}Pr_3$ amorphous ribbon. Therefore, it seems that the higher the GFA, the more topological type clusters in the Pr–Ni–Al amorphous alloys, on the contrary, the more chemical order type clusters, the lower the GFA.

Table 3. Gaussian decomposition results of RDFs of $Pr_{60}Ni_{30}Al_{10}$ BMA rod and $Al_{87}Ni_{10}Pr_3$ amorphous ribbon, r_{1p}, r_{2p}, r_{3p} denote the separated peak positions, atom correlations for each separated Gaussian peaks where C represents chemical order, T represents topological order and $s_i = \frac{\text{area of } i\text{th seperated Gaussian peak}}{\text{total area of the first three Gaussian peaks}} \times 100\%$

Amorphous alloys	1st separated Gaussian peak			2nd separated Gaussian peak			3rd separated Gaussian peak		
	r_{1p}/Å	s_1/%	correlation	r_{2p}/Å	s_2/%	correlation	r_{3p}/Å	s_3/%	correlation
$Pr_{60}Ni_{30}Al_{10}$	3.04	17.45	Pr–Ni (T)	3.68	75.00	Pr–Pr (T)	3.55	7.55	Al–Ni–Pr(C)
$Al_{87}Ni_{10}Pr_3$	2.35	16.98	Al–Al (C)	2.87	56.20	Al–Al (T)	3.45	26.82	Al–Ni (C)

4. Conclusions

In the present study, investigations on structure, superheated viscosity and crystallization are conducted for $Pr_{60}Ni_{30}Al_{10}$ BMA rods and $Al_{87}Ni_{10}Pr_3$ amorphous ribbons, and the relevant parameters and their relations are also analysed. The main results obtained are listed as follows.

1) The amorphous structure parameters are calculated from the XRD data, MRO is 4.21 Å in $Al_{87}Ni_{10}Pr_3$ amorphous ribbons. The nearest-neighbour atom distance r_1, average atom distance of displacement ρ, relative cluster radius r_c, atomic number of relative cluster N_c and coordination number of nearest-neighbour atoms N_1 of $Pr_{60}Ni_{30}Al_{10}$ BMA alloy are all bigger than those of $Al_{87}Ni_{10}Pr_3$.

2) $Pr_{60}Ni_{30}Al_{10}$ BMA rod has a very high GFA. The result of apparent crystallization energy E_x agree well with that of the amorphous structure parameter σ, indicating that $Pr_{60}Ni_{30}Al_{10}$ BMA rod has a more thermal stability than that of $Al_{87}Ni_{10}Pr_3$ amorphous ribbon.

3) The viscosity of $Pr_{60}Ni_{30}Al_{10}$ alloy is higher than that of $Al_{87}Ni_{10}Pr_3$ at the same superheating temperature, and the calculated diffusivity is the inverse of viscosity in relationship. The normalized value of E_{vPrE} is 2.312 eV which is about sixteen times bigger than that of $Al_{87}Ni_{10}Pr_3$. The high viscosity and relatively low diffusivity contribute significantly to high GFA of $Pr_{60}Ni_{30}Al_{10}$ alloy.

4) RDF Gaussian decompositions reveal that there are mainly Pr–Pr, Pr–Ni topological SRO and Al–Ni–Pr chemical SRO clusters in $Pr_{60}Ni_{30}Al_{10}$ BMA rod. In $Al_{87}Ni_{10}Pr_3$ amorphous ribbon, Al–Al topological and chemical SRO, Al–Ni chemical SRO and MRO clusters are the main structure compositions, which agrees well with the crystallization result. The higher the GFAs, the more topological SRO clusters in the Pr-Ni-Al amorphous alloys. The GFAs of the present glass-forming alloys are closely related to their structures.

Acknowledgment

The authors wish to thank Professor Wang Wei-Min for helpful discussion.

References

[1] Li Z, Bai H Y, Zhao D Q, Pan M X, Wang W L and Wang W H 2003 *Acta Phys. Sin.* **50** 652 (in Chinese)
[2] Zhao Z F, Zhang Z, Li Z, Wen P, Zhao D Q, Pan M X, Wang W L and Wang W H 2004 *Acta Phys. Sin.* **53** 850 (in Chinese)
[3] Zhang Y, Tan H, Kong H Z, Yao B and Li Y 2003 *J. Mater. Res.* **18** 665
[4] Inoue A 1997 *Mater. Sci. Eng.* A **226–228** 357
[5] Inoue A 2000 *Acta Mater.* **48** 279
[6] Mukherjee S, Schroers J, Zhou Z, Johnson W L and Rhim W K 2004 *Acta Mater.* **52** 3689
[7] Zhou J K, Bian X F, Wang W M, Xue X Y, Wang S H, Zhao Y and Yin K B 2004 *Mater. Lett.* **58** 2559
[8] Lupu N, McGreevy R L and Chiriac H 2004 *Mater. Sci. Eng.*A **375–377** 1105
[9] Warren W W 1991 *J. Non-Cryst. Solids* **135** 248
[10] Elliott S R 1991 *Nature* **354** 445
[11] Johnson W L 1999 *Bulk Metallic Glasses,* MRS Symposium Proceedings, Materials Research Society **54** 311 (Warrendale, PA)
[12] Sutherland W 1905 *Phil. Mag.* **9** 781
[13] Angel C A 1995 *Science* **267** 1924
[14] Busch R, Bakke E and Johnson W L 1998 *Acta Mater.* **46** 4725

[15] Fan G Y, Fech G J and Lavernia E J 2004 *Appl. Phys. Lett.* **84** 487
[16] Cohen M H and Grest G S 1979 *Phys.* **20** 1077
[17] Vertman A A and Samarin A M 1969 *Metody Issledovaniya Svoisty Metallicheskikh Rasplavov* (Moscow: Nauka)
[18] Waseda Y 1980 *The Structure of Non-crystalline Materials—Liquids and Amorphous Solids* (New York: McGraw-Hill)
[19] Qin J Y, Bian X F, Sliusarenko S I and Wang W M 1998 *J. Phys. Condens. Matter.* **14** 9
[20] Kr ü ger M, Soltwisch M, Petscherizin I and Quitmann D 1992 *J. Chem. Phys.* **96** 7352
[21] Hoyer W and Jodicke R 1995 *J. Non-cryst. Solids* **102** 192
[22] Fan G J, Löser W, Roth S, Eckert J and Schultz L 2000 *J. Mater. Res.* **15** 1556
[23] Suzuka N, Satoru M and Kazutaka T 2002 *J. Crystal Growth* **237** 1667
[24] Iida T and Guthrie I C R 1993 *The Properties of Liquid Metals* (Oxford: Clarendon Press) p217
[25] Wang H R, Ye Y F, Zhang J Y, Teng X Y, Min G H, Shi Z Q and Tian X L 2002 *Chin. Phys.* **11** 594
[26] Steinbery J,Tyagi S and Lord A E Jr. 1981 *Acta Metall.* **29** 1309
[27] Lu Z P and Liu C T 2002 *Acta Mater.* **50** 3501
[28] Kissinger H E 1956 *J. Res. Natl. Bur. Stan.* **57** 217
[29] Zhuang Y X, Wang W H, Zhang Y, Pang M X and Zhao D Q 1999 *Appl. Phys. Lett.* **75** 2394
[30] Zhou F G, Ni J X and Zhu H J 1989 *Application Mathematical and Physical Statistics* (Beijing: China Renmin University Press)
[31] Kita Y, Van Z J B and Morita Z 1994 *J. Phys.: Condens. Matter* **6** 811
[32] Wang W M, Bian X F, Qin J Y, Zhang L and Ye Y F 1999 *Science in China,* Ser E **29** 481(in Chinese)